FRAMELET-BASED MULTIRESOLUTION IMAGE FUSION WITH AN IMPROVED INTENSITY-HUE-SATURATION TRANSFORM

M. J. Choi *, D. H. Lee, H. S. Lim

Satellite Information Research Institute, KARI, 45, Eoeun-dong, Yuseong-gu, Daejeon, 305-333, KOREA
prime, dhlee - hslim@kari.re.kr

WG VII/6 – Remote Sensing Data Fusion

KEY WORDS: Satellite remote sensing, Pan-sharpening, Intensity-Hue-Saturation transform, Wavelets, Framelets, IKONOS imagery.

ABSTRACT:

The fusion of the panchromatic (PAN) image with multispectral (MS) images is a very useful tool for remote sensing applications that require both high-spatial and high-spectral resolution. A hybrid fusion method, which comprises of the standard intensity-hue-saturation (IHS) transform and a wavelet transform, was recently introduced in the literature. The hybrid fusion method was able to eliminate drawbacks of the IHS and wavelet-based methods, while keeping the advantages. In this paper, we introduce a new hybrid fusion method based on the fast IHS transform with a control parameter along with the framelet transform. The control parameter is used to minimize the radiance difference between the PAN image and the intensity image. In addition, the framelet transform, which is a natural generalization of orthonormal wavelets if redundancy is introduced into the wavelet system, is used to extract the detailed spatial information from the difference image of the PAN image and the intensity image. In order to verify the performance of the proposed method, an IKONOS PAN image with MS images were used. The proposed method produces more satisfactory results, both visually and quantitatively.

1. INTRODUCTION

Due to the technical limitation, most earth observe satellites, such as the SPOT, IKONOS, QuickBird, and KOMPSAT-2, provide a bundle of multispectral (MS) images at a lower spatial resolution and a panchromatic (PAN) image at a higher spatial resolution, instead of MS images at a high spatial resolution. Therefore, a pan-sharpening technique is very useful tool for remote sensing applications that require both high-spatial and high-spectral resolution (Zhang,2004).

Many image fusion techniques and software tools have been developed for specific applications. Of the hundreds of varied image fusion techniques, the best known methods are the intensity-hue-saturation (IHS) transform, principal component analysis, arithmetic combinations, and wavelet-based fusion methods. However, most of the existing techniques which perform suitably well with medium-resolution images, cannot always satisfy the fusion of MS and PAN high resolution images.

Recently, González-Audícana *et al.* (2004) introduced a hybrid fusion method comprised of the standard IHS transform and an undecimated discrete wavelet transform (UDWT). The hybrid fusion method was able to eliminate drawbacks of the IHS and wavelet-based methods, while keeping the advantages. Nevertheless, it is not efficient enough to quickly merge massive volumes of data from high-resolution satellite images because of its high computational complexity.

To reduce the computational cost, a fast IHS (FIHS) transform introduced by Tu *et al.*(2004) is employed on a new hybrid fusion method. Aside from its fast computing capability for fusing images, this method can extend traditional three-order transformations to an arbitrary order. In addition, we employed a framelet transform which is a natural generalization of orthonormal wavelets if redundancy is introduced into the wavelet system. It thereby avoids some of artifacts that arise when the decimated discrete wavelet transform is applied to the image fusion like the UDWT. Moreover, it can reduce the computational cost to a half of that of the UDWT.

More importantly, the proposed hybrid method enables us to reduce the overall computational cost to a half one again through simplifying the original mathematical model. A detailed explanation will be given later in the body of this paper.

On the other hand, one of disadvantages of IHS-based methods is that they destroy the spectral characteristics of the MS data (Choi,2006). Recent studies have shown that the large difference between the values of the PAN and intensity images appears to cause the large spectral distortion of fused MS images. Indeed, this difference (PAN-I) causes the altered saturation component in the RGB-IHS conversion model. Therefore, a FIHS transform with a control parameter is employed to minimize the radiance difference between the PAN image and the intensity image.

In order to verify the performance of the proposed method, an IKONOS PAN image with MS images were used. Then the spatial and spectral quality of the resulting images were analyzed and compared to images obtained from other well-known methods. The following chapter will explain the theory of the framelet transform. Readers unfamiliar with the wavelet theory are advised to continue to the third chapter, which the

* Corresponding author.

proposed method will be explained. The fourth chapter will present the experimental results.

2. THE FRAMELET TRANSFORM

As it is well known, except for the Haar filterbank, two-band finite impulse response (FIR) orthogonal filterbanks do not allow for symmetry. In addition, imposition of orthogonality for the two-band FIR filterbanks requires relatively long filter support for such properties as a high level of smoothness in the resulting scaling function and wavelets, as well as a high approximation order. Symmetry and orthogonality can both be obtained if the filterbanks have more than two bands. Furthermore, due to the critical sampling, orthogonal filters suffer a pronounced lack of shift invariance, though the desirable properties can be achieved through the design of tight frame filterbanks, of which orthogonal filters are a special case. In contrast to orthogonal filters, tight frame filters have a level of redundancy that allows for the approximate shift invariance behavior caused by the dense time-scale plane. Besides producing symmetry, the tight frame filterbanks are shorter and result in smoother scaling and wavelet functions. Before proceeding further, let me describe the basic concepts of frame theory and oversampled filterbanks

2.1 A Tight Wavelet Frame

A set of functions $\{\psi^1,\ldots,\psi^{N-1}\}$ in a square integrable space, $L^2(\square)$, is called a frame if there exist $A>0$, $B<\infty$ so that, for any function $f\in L^2(\square)$,

$$A\|f\|^2 \le \sum_{i=1}^{N-1}\sum_{j\in\square}\sum_{k\in\square}\left|\left\langle f,\psi^i(2^j\cdot-k)\right\rangle\right|^2 \le B\|f\|^2, \qquad (1)$$

where A and B are known as frame bounds, $\langle f,g\rangle := \int_{\square} f(x)\overline{g(x)}\,dx$, and $\|f\|^2 := \langle f,f\rangle$.

The special case of $A=B$ is known as tight frame. In a tight frame we have, for all $f\in L^2(\square)$,

$$\sum_{i=1}^{N-1}\sum_{j\in\square}\sum_{k\in\square}\left|\left\langle f,\psi^i(2^j\cdot-k)\right\rangle\right|^2 = A\|f\|^2$$

which implies

$$f = A^{-1}\sum_{i=1}^{N-1}\sum_{j\in\square}\sum_{k\in\square}\left\langle f,\psi^i(2^j\cdot-k)\right\rangle\psi^i(2^j\cdot-k).$$

In order to have a fast wavelet frame (or framelet) transform, multiresolution analysis is generally used to derive tight wavelet frames from scaling functions.

Now, we obtain the following spaces:

$$V_j = \operatorname*{Span}_k\{\phi(2^j t-k)\}$$
$$W_{i,j} = \operatorname*{Span}_k\{\psi^i(2^j t-k)\},\quad i=1,\ldots,N-1$$
with
$$V_j = V_{j-1}\cup W_{1,j-1}\cup W_{2,j-1}\cup\cdots\cup W_{N-1,j-1},$$

and the corresponding scaling function and wavelets satisfy the following multiresolution equations:

$$\phi(t) = \sqrt{2}\sum_k h_0(k)\phi(2t-k)$$
$$\psi^i(t) = \sqrt{2}\sum_k h_i(k)\phi(2t-k),\quad i=1,\ldots,N-1.$$

Now, the frame bound A takes on the value

$$A = \frac{1}{2}\sum_{i=0}^{N-1}\|h_i\|^2 .$$

2.2 Oversampled Filterbanks

The frame condition can be expressed in terms of oversampled polyphase filters. Given a set of N filters, we define them in terms of their polyphase components:

$$H_i(z) = H_{i,0}(z^2) + z^{-1}H_{i,1}(z^2),\quad i=0,\ldots,N-1,$$

where

$$H_{i,l}(z) = \sum_n h_i(2n-l)z^{-n},\ l=0,1.$$

Now define the polyphase analysis matrix as

$$\mathrm{H}(z) = \begin{pmatrix} H_{0,0}(z) & H_{0,1}(z)\\ H_{1,0}(z) & H_{1,1}(z)\\ \vdots & \vdots\\ H_{N-1,0}(z) & H_{N-1,1}(z)\end{pmatrix}.$$

If we now define the signal $X(z)$ in terms of its polyphase components, we then have

$$\mathrm{x}(z) = (X_0(z)\ \ X_1(z))^T,$$

where the equation $X_l(z),\ l=0,1$ is defined in terms of the time domain signal, $x(n)$, as follows:

$$X_l(z) = \sum_n x(2n-l)z^{-n}.$$

The overall output signal $\hat{X}(z)$ of the analysis-synthesis filterbank can be expressed as

$$\hat{X}(z) = (1 \;\; z^{-1})\mathrm{H}^T(z^2)\mathrm{H}(z^{-2})\mathrm{x}(z^2) .$$

Furthermore, to meet perfect reconstruction (PR) condition $\hat{X}(z) = X(z)$, we require that $\mathrm{H}^T(z)\mathrm{H}(z^{-1}) = \mathrm{I}$.

Selesnick (2004), on the other hand, shows that a three-band tight frame filterbank PR conditions can be expressed in terms of the Z -transforms of the filters h_0 , h_1 , and h_2 . Moreover, the PR conditions can be easily extended to N filters downsampled by 2:

$$\sum_{i=0}^{N-1} H_i(z)H_i(z^{-1}) = 2$$

$$\sum_{i=0}^{N-1} H_i(-z)H_i(z^{-1}) = 0$$

Last, Chui et al. (2000) show a necessary condition for the filterbank to exist. That is, the filters $H_i(z),\ i = 0,\ldots,N-1$ must each satisfy the following inequality:

$$\left|H_i(z)\right|^2 + \left|H_i(-z)\right|^2 < 2, \quad |z| = 1 .$$

Notice that the equality reduces to the traditional case of a two-band orthogonal filterbank.

2.3 A Symmetric Tight Wavelet Frame with Two Generators

In this section, we introduce the construction of a symmetric tight wavelet frame with two generators based on a three-band tight frame filterbank and provide a result and an example (Selesnick, 2004).

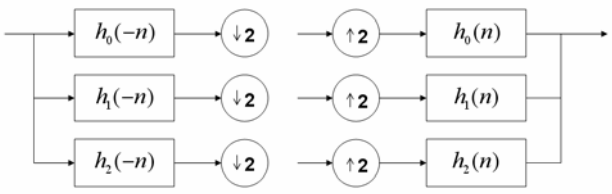

Figure 1. A three-band PR filterbank

2.3.1 PR Conditions and Symmetry Condition: The PR conditions for the three-band filterbank, which are illustrated in Fig. 1, can be obtained by setting the N in the section 2.2. to a value of 3. That is, we have the following two equations:

$$\sum_{i=0}^{2} H_i(z)H_i(z^{-1}) = 2 \qquad (2)$$

$$\sum_{i=0}^{2} H_i(-z)H_i(z^{-1}) = 0 . \qquad (3)$$

The PR conditions can also be written in matrix form as

$$\mathrm{H}^T(z)\mathrm{H}(z^{-1}) = \mathrm{I} \qquad (4)$$

where

$$\mathrm{H}(z) = \begin{pmatrix} H_{0,0}(z) & H_{0,1}(z) \\ H_{1,0}(z) & H_{1,1}(z) \\ H_{2,0}(z) & H_{2,1}(z) \end{pmatrix} .$$

Also, if $h_0(n)$ is compactly supported, then a solution $\{ h_1(n) , h_2(n) \}$ to Eq. (4) exists if and only if

$$\left|H_0(z)\right|^2 + \left|H_0(-z)\right|^2 < 2, \quad |z| = 1 . \qquad (5)$$

A wavelet tight frame with only two symmetric or anti-symmetric wavelets is generally impossible to obtain with a compactly supported symmetric scaling function, $\phi(t)$. However, Petukhov (2003) states a condition that the lowpass filter $h_0(n)$ must satisfy so that this becomes possible. Therefore, if $h_0(n)$ is symmetric, compactly supported, and satisfies Eq.(5), then an (anti-)symmetric solution $\{ h_1(n) , h_2(n) \}$ to Eq. (4) exists if and only if all the roots of

$$2 - H_0(z)H_0(z^{-1}) - H_0(-z)H_0(-z^{-1}) \qquad (6)$$

have even multiplicity.

2.3.2 Case $H_2(z) = H_1(-z)$: The goal is to design a set of three filters that satisfy the PR conditions in which the lowpass filter, $h_0(n)$, is symmetric and the filters $h_1(n)$ and $h_2(n)$ are each either symmetric or anti-symmetric. There are two cases. Case I denotes the case where $h_1(n)$ is symmetric and $h_2(n)$ is anti-symmetric. Case II denotes the case where $h_1(n)$ and $h_2(n)$ are both anti-symmetric. The symmetry condition for $h_0(n)$ is

$$h_0(n) = h_0(N-1-n) , \qquad (7)$$

where N is the length of the filter $h_0(n)$.

We dealt only with Case I of even-length filters. Solutions for Case I can be obtained from solutions where $h_2(n)$ is a time-reversed version of $h_1(n)$ (and where neither filter is (anti-) symmetric).

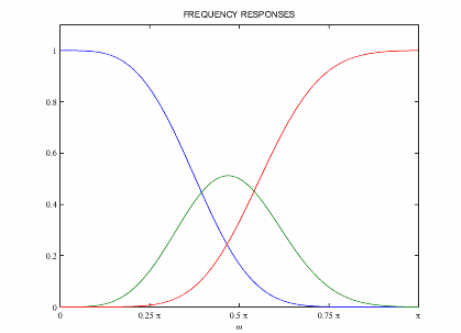

Figure 2. The frequency responses of h_0, h_1, and h_2 in the example

To show this, suppose that $h_0(n)$, $h_1(n)$, and $h_2(n)$ satisfy the PR conditions and that

$$h_2(n) = h_1(N-1-n)\,. \tag{8}$$

Then, by defining

$$h_1^{new}(n) = \frac{1}{\sqrt{2}}\big(h_1(n) + h_2(n-2d)\big), \tag{9}$$

$$h_2^{new}(n) = \frac{1}{\sqrt{2}}\big(h_1(n) - h_2(n-2d)\big) \text{ with } d \in \mathbf{Z}\,, \tag{10}$$

the filters h_0, h_1^{new}, and h_2^{new} also satisfy the PR conditions, and h_1^{new}, h_2^{new} are symmetric and anti-symmetric as follows:

$$h_1^{new}(n) = h_1^{new}(N_2 - 1 - n)\,,$$
$$h_2^{new}(n) = -h_2^{new}(N_2 - 1 - n)\,,$$

where $N_2 = N + 2d$.

We state main results of the paper (Selesnick, 2004) without the proof. The filters h_0, h_1, and h_2 with symmetries Eq. (7) and Eq. (8) satisfy the PR conditions if their polyphase components of the filters are given by

$$H_{0,0}(z) = z^{-M/2}\sqrt{2}A(z)B(z^{-1}), \tag{11}$$
$$H_{1,0}(z) = A^2(z), \tag{12}$$
$$H_{1,1}(z) = -B^2(z), \tag{13}$$

where

$A(z)A(z^{-1}) = 0.5 + 0.5U(z)$,

$B(z)B(z^{-1}) = 0.5 - 0.5U(z)$,

$U(z)U(z^{-1}) = 1 - 2H_{0,0}(z)H_{0,0}(z^{-1})$, and $M = N/2 - 1$.

2.3.3 Filter Design: First, obtain a lowpass filter, $h_0(n)$, which has an even-length and which satisfies the symmetry condition of Eq. (6). The design procedure is as follows:

1) Knowing $H_0(z)$ and, thus $H_{0,0}(z)$, use spectral factorization to find $U(z)$ from $1 - 2H_{0,0}(z)H_{0,0}(z^{-1})$.
2) Find $A(z)$ and $B(z)$ from $H_{0,0}(z)$ and $U(z)$ by using factorization and root selection.
3) Find $H_{1,0}(z)$ and $H_{1,1}(z)$ by using Eq. (12) and Eq. (13), respectively.
4) Find $H_1(z)$ and $H_2(z)$ by using $H_{1,0}(z)$, $H_{1,1}(z)$ and Eq. (8).
5) Obtain (anti-) symmetric wavelets h_1 and h_2 by using Eq. (9) and Eq. (10).

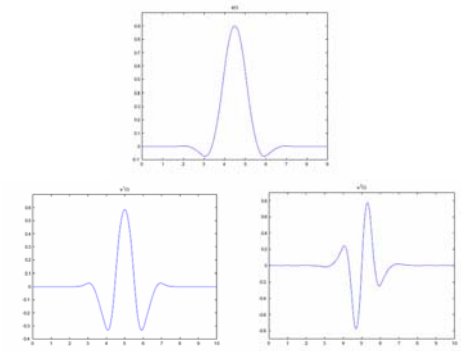

Figure 3. The symmetric scaling function, $\phi(t)$, and the two wavelets $\psi^1(t)$ and $\psi^2(t)$ of the example

n	$h_0(n)$	$h_1(n)$	$h_2(n)$
0	0.00069616789827	-0.00014203017443	0.00014203017443
1	-0.02692519074183	0.00549320005590	-0.00549320005590
2	-0.04145457368920	0.01098019299363	-0.00927404236573
3	0.19056483888763	-0.13644909765612	0.07046152309968
4	0.58422553883167	-0.21696226276259	0.13542356651691
5	0.58422553883167	0.33707999754362	-0.64578354990472
6	0.19056483888763	0.33707999754362	0.64578354990472
7	-0.04145457368920	-0.21696226276259	-0.13542356651691
8	-0.02692519074183	-0.13644909765612	-0.07046152309968
9	0.00069616789827	0.01098019299363	0.00927404236573
10	0	0.00549320005590	0.00549320005590
1	0	-0.00014203017443	-0.00014203017443

Table 1. Coefficients for the example

2.3.4 Example: To obtain a lowpass filter, $h_0(n)$, with a minimal length, we used a maximally flat lowpass even-length FIR filter with the following transfer function :

$$F_{m,n}(z) = \left(\frac{1+z^{-1}}{2}\right)\left(\frac{z+2+z^{-1}}{4}\right)^m \sum_{k=0}^{n}\binom{m+k-0.5}{k}\left(\frac{-z+2-z^{-1}}{4}\right)^k.$$

Unfortunately, although the setting of $H_0(z) := F_{m,n}(z)$ gives an $H_0(z)$ that does not satisfy Eq. (6), we can use a linear combination of various $F_{m,n}(z)$ values to obtain a $H_0(z)$ filter that does satisfy Eq. (6). For example, if we use a setting of

$$H_0(z) = z^{-4}\sqrt{2}\big(\alpha F_{2,1}(z) + (1-\alpha)F_{3,1}(z)\big)\,, \tag{14}$$

then, for special values of α, $H_0(z)$ satisfies Eq. (6).

Figure 2 shows the filters for α = 1.0720. Figure 3 shows the resulting scaling function and wavelets. Table I lists the coefficients of the filters h_0 , h_1 and h_2 .

2.3.5 Two-Dimensional Extension: The 2D extension can be obtained by alternating between rows and columns, as is usually done for typical discrete wavelet transforms. The corresponding filter bank, which is illustrated in Fig.4, is iterated on the lowpass branch (the first branch).

3. THE PROPOSED FUSION METHOD

To apply any of the methods of image fusion described in this paper, the MS image and the PAN image must be accurately superimposed. Thus, both images must be co-registered, and the MS image resampled to make its pixel size the same as the PAN image. In order to achieve this, a robust registration technique and a bi-cubic interpolator were used.

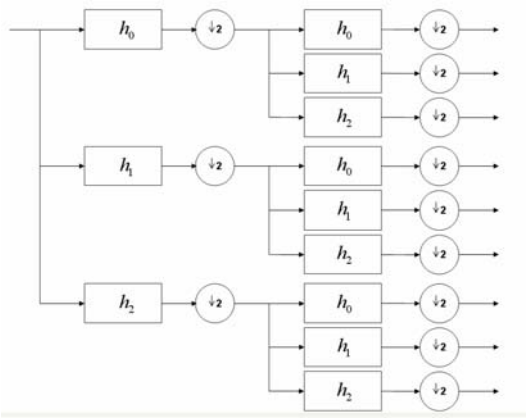

Figure 4. An oversampled filterbank for a 2-D image

3.1 FIHS Fusion Method

The FIHS fusion for each pixel can be formulated by the following procedure (Tu *et al.*, 2001):

$$\begin{bmatrix} F(R) \\ F(G) \\ F(B) \end{bmatrix} = \begin{bmatrix} R + (PAN - I) \\ G + (PAN - I) \\ B + (PAN - I) \end{bmatrix}, \quad (15)$$

where $F(X)$ is the fused image of the X band, for X = R, G, and B, respectively.

3.2 The Hybrid Method proposed by González-Audícana *et al.*

A multiresolution wavelet decomposition is used to execute the detailed extraction phase, and the IHS procedure is followed to inject the spatial detail of the PAN image into the MS image. In other words, instead of using the PAN image in Eq. (15), the results of the PAN image and the intensity image fused by the substitutive wavelet method is used. The fusion results of the PAN image and the intensity image are expressed as follows:

$$I_{new} = I_r + \sum_{k=1}^{n} W_{PAN_k}, \quad (16)$$

where I_r is the low-frequency version of the wavelet-transformed intensity image and $\sum_{k=1}^{n} W_{PAN_k}$ is the sum of high-frequency versions of the wavelet-transformed PAN image.

3.3 The Proposed Hybrid Method

Assume that, without the loss of generality, the hybrid method is based on the FIHS fusion method instead of on the traditional IHS method. This is because Eq. (15) holds.

The hybrid method can be simplified with the following procedure:

$$\begin{bmatrix} F(R) \\ F(G) \\ F(B) \end{bmatrix} = \begin{bmatrix} R + (I_{new} - I) \\ G + (I_{new} - I) \\ B + (I_{new} - I) \end{bmatrix} = \begin{bmatrix} R + \sum_{k=1}^{n} W_{(PAN-I)_k} \\ G + \sum_{k=1}^{n} W_{(PAN-I)_k} \\ B + \sum_{k=1}^{n} W_{(PAN-I)_k} \end{bmatrix}, \quad (17)$$

where $\sum_{k=1}^{n} W_{(PAN-I)_k}$ is the sum of the high-frequency versions of the wavelet-transformed difference image of the PAN image and the I image.

As a result, we easily obtained fused images with the fast scheme of the hybrid method: We simply added to each MS image the detailed information extracted from the difference image of the PAN image and the intensity image. Therefore, the proposed hybrid method is much simpler and faster than the hybrid method.

3.4 IKONOS Pan-sharpening Technique

When IHS-like fusion methods are used with IKONOS imagery, there is a significant color distortion, due primarily to the extensive range of wavelengths in an IKONOS PAN image. This difference obviously induce the color distortion problem in IHS fusion as a result of the mismatch; that is, the PAN image and the intensity image are spectrally dissimilar. To minimize the radiance differences between the I image and the PAN image, Tu *et al.* (2004) introduced the near-infrared (NIR) band with spectral adjustment applied to the I image, considering that

$$I' = \frac{R + a * G + b * B + NIR}{3}, \quad (18)$$

where a and b are weighting parameters defined to take into account that the spectral response of the PAN image does not cover that of the blue and green band. The value of these parameters was estimated experimentally after the fusion of 92 IKONOS images, covering different areas. According to the experimental results obtained by Tu *et al.* (2004), the best

weighting parameters of a and b for G and B bands are 0.75 and 0.25, respectively.

However, since the above two weighting parameters are totally depends on the IKONOS imagery, these parameters cannot be applied to other satellite image fusion. Therefore, a control parameter, β, will additionally be suggested in this paper. This will be selected when the mean value of the difference between the PAN image and the $\beta * \mathrm{I}'$ image is a minimum, so as to minimize the radiance difference between two images.

The proposed hybrid method for IKONOS image fusion is as follows:

$$\begin{bmatrix} F(R) \\ F(G) \\ F(B) \\ F(NIR) \end{bmatrix} = \begin{bmatrix} \mathrm{R} + \sum_{k=1}^{n} W_{(\mathrm{PAN}-\beta * \mathrm{I}')_k} \\ \mathrm{G} + \sum_{k=1}^{n} W_{(\mathrm{PAN}-\beta * \mathrm{I}')_k} \\ \mathrm{B} + \sum_{k=1}^{n} W_{(\mathrm{PAN}-\beta * \mathrm{I}')_k} \\ \mathrm{NIR} + \sum_{k=1}^{n} W_{(\mathrm{PAN}-\beta * \mathrm{I}')_k} \end{bmatrix}. \quad (19)$$

In sum, we employed the FIHS method in order to reduce the computational cost of the original hybrid method along with the simplification of the mathematical model, and suggested the control parameter and the framelet transform in order to enhance the overall performance of the fused images.

4. EXPERIMENTAL STUDY AND ANALYSIS

To verify the performance of the proposed method, an IKONOS PAN image and MS images of the Korean city of Daejeon, which were acquired on 9 March 2002, were used. The IKONOS imagery contains a 1m PAN image and four-band 4 m MS images. The data for this experiment comprised a PAN image and four R, G, B, and NIR MS images.

Table 2. Comparison of IKONOS Fusion Results

		eIHS	eSW-Wavelets	eSWI-Trous	eFSWI-Framelets
bias (%) (ideal value: 0)	R	16.68	0.00	0.00	0.00
	G	16.87	0.00	0.00	0.00
	B	18.85	0.00	0.00	0.00
	NIR	18.81	0.00	0.00	0.00
CC (ideal value: 1)	R	0.95	0.96	0.97	0.97
	G	0.95	0.96	0.97	0.97
	B	0.93	0.95	0.96	0.96
	NIR	0.94	0.95	0.96	0.96
SD (%) (ideal value: 0)	R	10.78	9.53	8.51	8.36
	G	10.39	8.62	7.84	7.66
	B	12.12	10.18	9.29	9.15
	NIR	11.27	10.13	8.77	8.79
sCC	R	0.99	0.94	0.98	0.98
	G	0.99	0.94	0.98	0.98
	B	0.99	0.93	0.98	0.98
	NIR	0.98	0.95	0.98	0.98
ERGAS		5.26	2.41	2.15	2.12
SAM(deg.)		3.71	3.42	3.10	3.09
Q4		0.58	0.92	0.94	0.94

In order to assess the quality of the fused MS images, reference MS images with the same spatial resolution as the PAN image were needed. However, since such MS images were unavailable, spatially degraded PAN and MS images, which were generated by a lowpass filtering and sub-sampling procedure, were considered (Wald *et al.*, 1997).

4.1 The Quality Indices for Quantitative Analysis

The spectral and spatial quality indices for quantitative analysis have been used in (Ranchin *et al.*,2000; Alparone *et al.*, 2004): namely, the bias; the standard deviation (SD); the correlation coefficient (CC); the relative global dimensional synthesis error, which is known as *the erreur relative globale adimensionelle de synthése* (ERGAS); the spectral angle mapper (SAM); the global quality index, Q4; and the spatial correlation index proposed by Zhou *et al.* (sCC).

Note that the bias, SD, CC, ERGAS, SAM and Q4 are applied at degraded scale, but sCC is applied only at full scale without any degradation.

4.2 Quantitative Analysis

Table 2 shows the results of a comparative analysis of the IKONOS image fusion with the seven quality indices.

The comparison presented in Table 2 shows that the extended IHS method (eIHS) has lower CC and Q4 values but greater bias, SD, ERGAS, SAM values than the extended substitutive wavelet method (eSW-Wavelets). Therefore, the spectral quality of the images fused by the eSW-Wavelets method is greater than that of the images fused by the eIHS method. However, since the sCC values of the eIHS method are greater than those of the eSW-Wavelets, the spatial quality of the images fused by the eIHS method is greater than that of the images fused by the eSW-Wavelets.

On the other hand, the hybrid method between the eIHS and eSW methods (eSWI-Trous) has lower bias, SD, ERGAS, and SAM values but greater CC, sCC and Q4 values than both the eIHS and the eSW methods. Consequently, the spatial and spectral quality of the images fused by the eSWI-Trous method is greater than those of the images fused by both the eIHS and the eSW methods. That is to say, the hybrid fusion method was able to eliminate drawbacks of the IHS and wavelet-based methods, while keeping the advantages.

In addition, Table 2 shows that the proposed fast hybrid method (eFSWI-Framelets) has lower bias, SD, ERGAS, and SAM values but greater CC, sCC and Q4 values than the eSWI-Trous method. Therefore, the spatial and spectral quality of the images fused by the eFSWI-Framelets method is greater than those of the images fused by the eSW-Trous method. This is why the control parameter and the framelet transform are suggested in this paper.

4.3 Visual Analysis

Figure 5 shows the results of full-scale visual fusion. For Fig. 5 (b), aliasing artifacts induced during the interpolation process are apparently visible. Such impairments disappear in images fused by the eIHS method and are easily explained by Eq. (15),

in which the aliasing patterns, present in MS images, and hence also in the intensity image, are cancelled when the intensity image is subtracted from each of the spectral bands. Similarly, the aliasing artifacts also disappear in images fused by the eSWI-Trous and the eFSWI-Framelets methods. However, the aliasing artifacts still appear in images fused by the eSW-Wavelets method. Consequently, the eIHS, the eSWI-Trous and the eFSWI-Framelets methods are more acceptable for visual analysis.

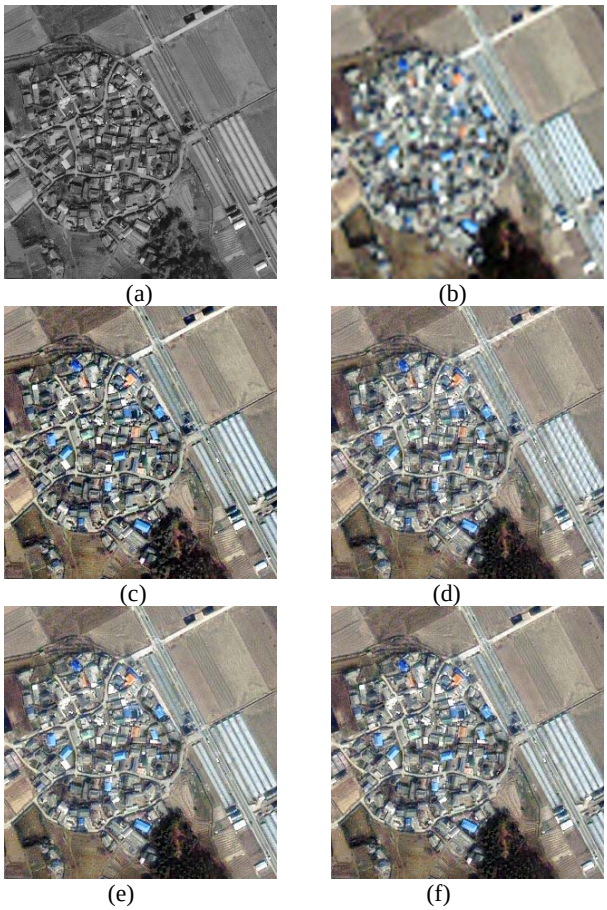

Figure 5. The results of full-scale visual fusion: (a) the PAN image; (b) the resampled original MS image; (c) fused by the eIHS; (d) fused by eSW-Wavelets; (e) fused by eSWI-Trous; (f) fused by the eFSWI-Framelets.

5. CONCLUSION

We present the new hybrid fusion method based on the FIHS transform with a control parameter along with the framelet transform, and validate this new approach by merging an IKONOS PAN image with MS images. To analyze the spatial and spectral quality of the resulting images, we used the seven quality indices, namely the bias, CC, SD, ERGAS, SAM, Q4, and sCC, and compared the results with the quality of images fused by other methods of image fusion. In sum, the proposed method produces more satisfactory results, both visually and quantitatively.

ACKNOWLEDGMENT

We would like to thank Prof. Paolo Gamba for supplying the quantitative evaluation programs which are provided by the IEEE GRSS DFTC, © L. Alparone.

REFERENCE

Alparone, L., Baroni, S., Garzelli, A., and Nencini, F.,2004. A Global Quality Measurement of Pan-Sharpened Multispectral Imagery. *IEEE GRSL*. 1(4), pp.313-317.

Choi, M.,2006. A New Intensity-Hue-Saturation Fusion Approach to Image Fusion With a Tradeoff Parameter. *IEEE TGRS*, 44(6), pp.1672-1682.

Chui, C. K., and He, W.,2000. Compactly supported tight frames associated with refinable functions. *ACHA*, 8, pp.293-319.

González-Audícana, M., Saleta, J. L., Catalan, R. G., and Garcia, R., 2004. Fusion of Multispectral and Panchromatic images Using Improved IHS and PAC mergers Based on Wavelet Decomposition. *IEEE TGRS*, 42(6), pp. 1291-1299.

Petukhov, A.,2003. Symmetric framelets. *Constructive Approximation*. 19(2), pp.309-328.

Ranchin, T. and Wald, L.,2000. Fusion of High Spatial and Spectral Resolution images: The ARSIS concept and Its Implementation. *PE&RS*. 66, pp.49-61.

Selesnick, I. W.,2004. Symmetric wavelet tight frames with two generators. *ACHA*, 17, pp.211-225.

Tu, T. M., Su, S. C., Shyn, H. C., and Huang, P. S.,2001. A new look at HIS-like image fusion methods. *Information Fusion*. 2(3), pp. 177-186.

Tu, T. M., Huang, P. S., Hung, C. L., and Chang. C.P.,2004. A Fast Intensity-Hue-Saturation Fusion Technique With Spectral Adjustment for IKONOS Imagery. *IEEE GRSL*, 1(4), pp. 309-312.

Wald, L., Ranchin, T., and Mangolini, M.,1997. Fusion of Satellite images of different spatial resolution: Assessing the quality of resulting images. *PE&RS*, 63(6), pp. 691-699.

Zhang, Y.,2004. Understanding Image Fusion. *PE&RS*, 70(6), pp.653-760.